CHARACTERIZATION OF HYBRID ROCKET INTERNAL HEAT FLUX AND 11'1'1'11 FUEL PYROLYSIS

L. D. Strand*, M. D. Jones†, and R L. Ray
Jet Propulsion Laboratory
California Institute of Technology
Pasadena, California

N. S. Cohen*
Cohen Professional Services
Redlands, California

Abstract

As an assistance in the development and verification of CFD models of the hybrid rocket ("pure" or "classic") combustion process, the objectives of this study were to bound the relative proportions of radiative and convective heat transfer to the solid fuel and to determine the pyrolysis law for hydroxyl-terminated polybutadiene (11'1'1'11) under hybrid heating conditions. Tests were carried out with a hybrid slab window motor, using several diagnostic techniques, over a range of motor pressure and oxidizer mass flux conditions. The results, for the most part, are consistent with turbulent boundary layer convective heat flux as the primary mechanism for driving regression rate. However, particle radiation from fine powdery soot is a significant heat flux contributor for pure 11'1'1'13 fuel, and should be accounted for in attempts to predict fuel regression rates and size-scaling effects.

Nomenclature

a_g	constant in the expression for gas emissivity
al,	constant in the expression for particle cloud emissivity
c_g	specific heat of combustion gases
C*	rocket motor characteristic velocity
G	total specific flow rate (or mass flux) through the port
G_{ox}	oxygen head end specific flow rate
L	radiation path length
N_p	particle number density
O/F	oxidizer to fuel ratio

* Associate Fellow AIAA
† Member AIAA

P	pressure (expressed in Psi for use with constants given)
Pr	Prandtl number
Q	heat flux
T_g	gas temperature
T_p	radiating particle temperature
T_s	surface temperature
x	distance from head end of fuel grain
α_p	weight fraction of radiating particles
ϕ	total heat flux
ϕ_c	convective heat flux
$\phi_{R,g}$	radiative heat flux from the gas
$\phi_{R,p}$	radiative heat flux from the particle cloud
μ_g	gas viscosity
σ	Stefan-Boltzman constant

Introduction

Hybrid propulsion is being considered for advanced launch vehicle applications due to the fact that it offers advantages of safety, low cost, environmentally benign combustion products, attractive performance and mission flexibility relative to current rocket boosters.[1-2] A limitation, however, of the "classic" hybrid rocket concept is the regression rate properties of the solid fuel. Regression rates tend to be low (an order of magnitude lower than solid propellant rates) and dependent upon the fuel grain geometry. This is because the rates are controlled by the fluid dynamics of the boundary layer established adjacent to the solid fuel surface - the location of the reactants mixing and combustion and the transfer of heat back to the fuel surface. These regression rate properties have an impact on the volumetric loading and utilization efficiency of the solid fuel.

After considerable work during the 1960's,[3] hybrid propulsion R&D has been virtually non-existent until recent years.[4] As a part of this renewed interest, JPL, under NASA sponsorship, has been conducting a hybrid fuel combustion research program to modernize or advance our state of knowledge of the combustion process as a means of overcoming the above regression rate limitations. The program has had three objectives:

Assist in the development of improved hybrid fuels[5]
Improve our understanding of the mechanisms controlling fuel regression rates[6,7]

Describe the operational characteristics, including combustion stability and size-scaling effects, of proposed hybrid propulsion concepts.[7,8]

As an assistance in the development of CFD models of the hybrid combustion process, specific objectives of the work reported here were to bound the relative proportions of radiative and convective heat transfer to the fuel surface in the developed boundary layer region and to determine the pyrolysis law for hydroxyl-terminated polybutadiene (HTPB) under hybrid rocket heating conditions.

Test Program

The studies were carried out using a hybrid slab window motor apparatus shown schematically in Figure 1. It consists of a (1) head-end closure, (2) flow straightener/igniter section with (3) flow straightening screens, (4) test section with quartz viewing ports, (5) aft combustor section, (6) aft closure with (7) graphite nozzle, (8) internal spacer to control burner cross-sectional area, (9) fuel casting base plate, and (10) fuel slab. Single (as shown) or opposed dual rectangular fuel slabs have been tested, with gaseous oxygen (GOX) as the oxidizer injectant. While adaptable to a variety of diagnostic measurement techniques, the apparatus is limited to internal pressures of less than 315 psi (2.2 MPa) and oxidizer head-end specific flow rates of less than 0.15 lbm/in^2-s (0.01 kg/cm^2-s). Measured motor pressure-oxidizer flux correlations for the family of nozzle throat diameters are shown in Figure 2. The apparatus has been described in greater detail in Reference 5.

Measurements made in the slab motor consisted of the following:

- fuel regression rates (average and local values as a function of motor axial position) and specific flow rates
- motor pressure
- injectant flow turbulence and roughness of combustion
- combustion efficiency
- extinguishability of gas-generator type hybrid fuels
- windowed high-speed video of the combustion process
- gas temperature and fuel surface temperature
- components of radiation and convective heat transfer

For the tests reported here the slab motor was instrumented per the respective test configurations shown in Figure 3. Configuration A consisted of heat flux measurements in the aft region of the motor with a calorimeter (total) and radiometer (radiation component). Configuration B used IR pyrometry to measure the core gas temperature and the combusting fuel surface temperature in the motor aft region. Configuration C combined A and B - calorimeter and radiometer measurements in the aft region and IR pyrometer measurements in the forward region of the motor.

Core gas temperature measurements were performed with a Mikron Series 77E 2-color infrared thermometer. The instrument has a field of view of 25 mm (1 inch) diameter and time response (zero to 95% of final value) of 40 ms. A Mikron Series M67S infrared thermometer was used for the combusting fuel surface temperature measurements. It operates at a narrow wavelength centered at 3.88 microns, which allowed viewing through the quartz window and penetration through the gaseous products of combustion. The field of view and time response are 25 mm and 100 ms, respectively.

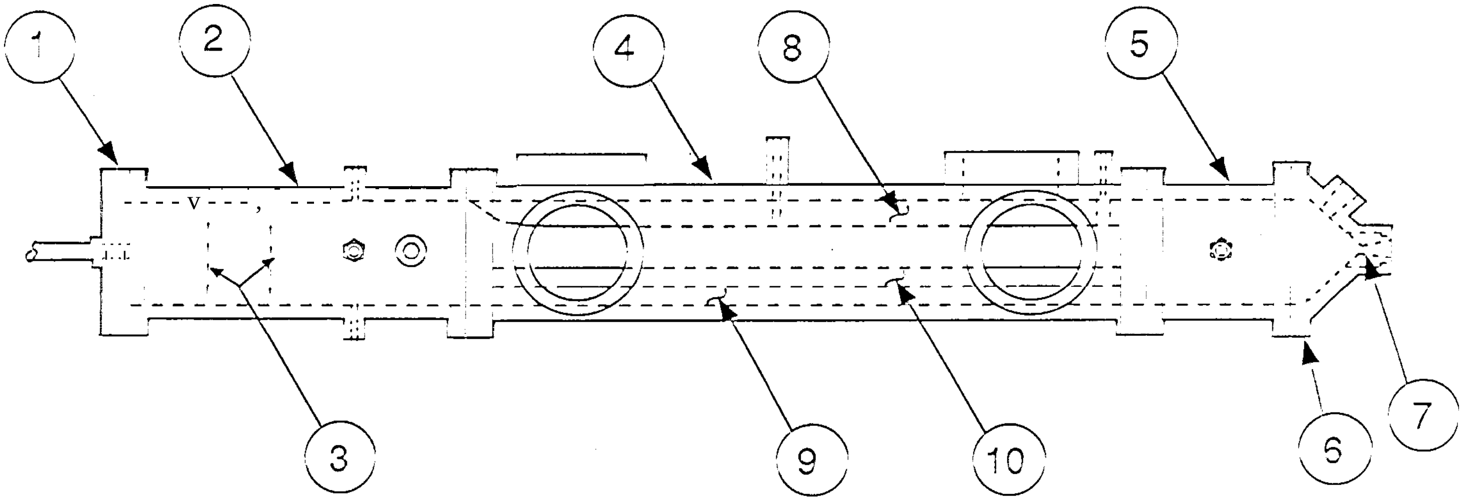

Fig. 1 Hybrid slab window motor

Fig. 2 Chamber pressure vs. Gox

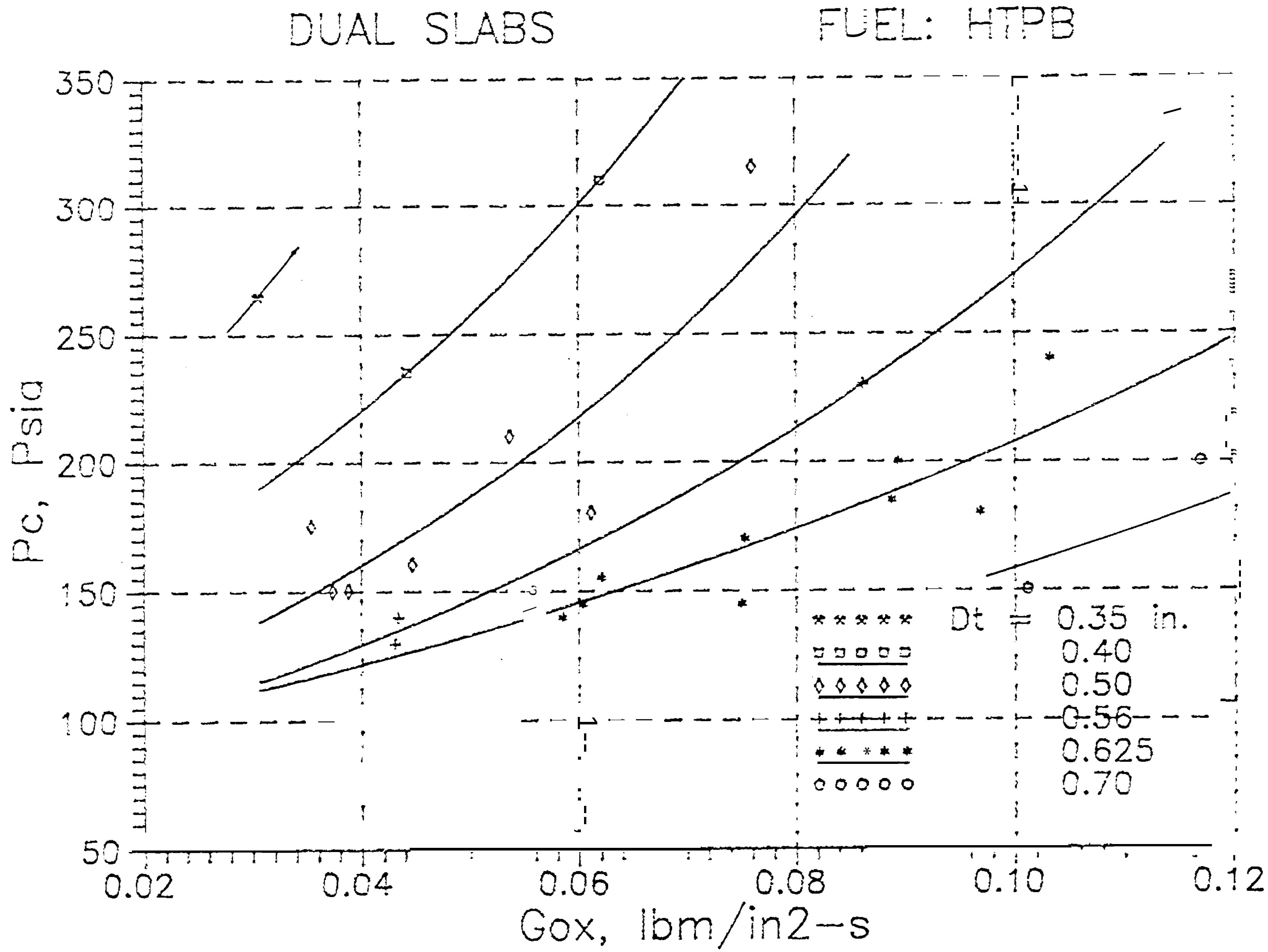

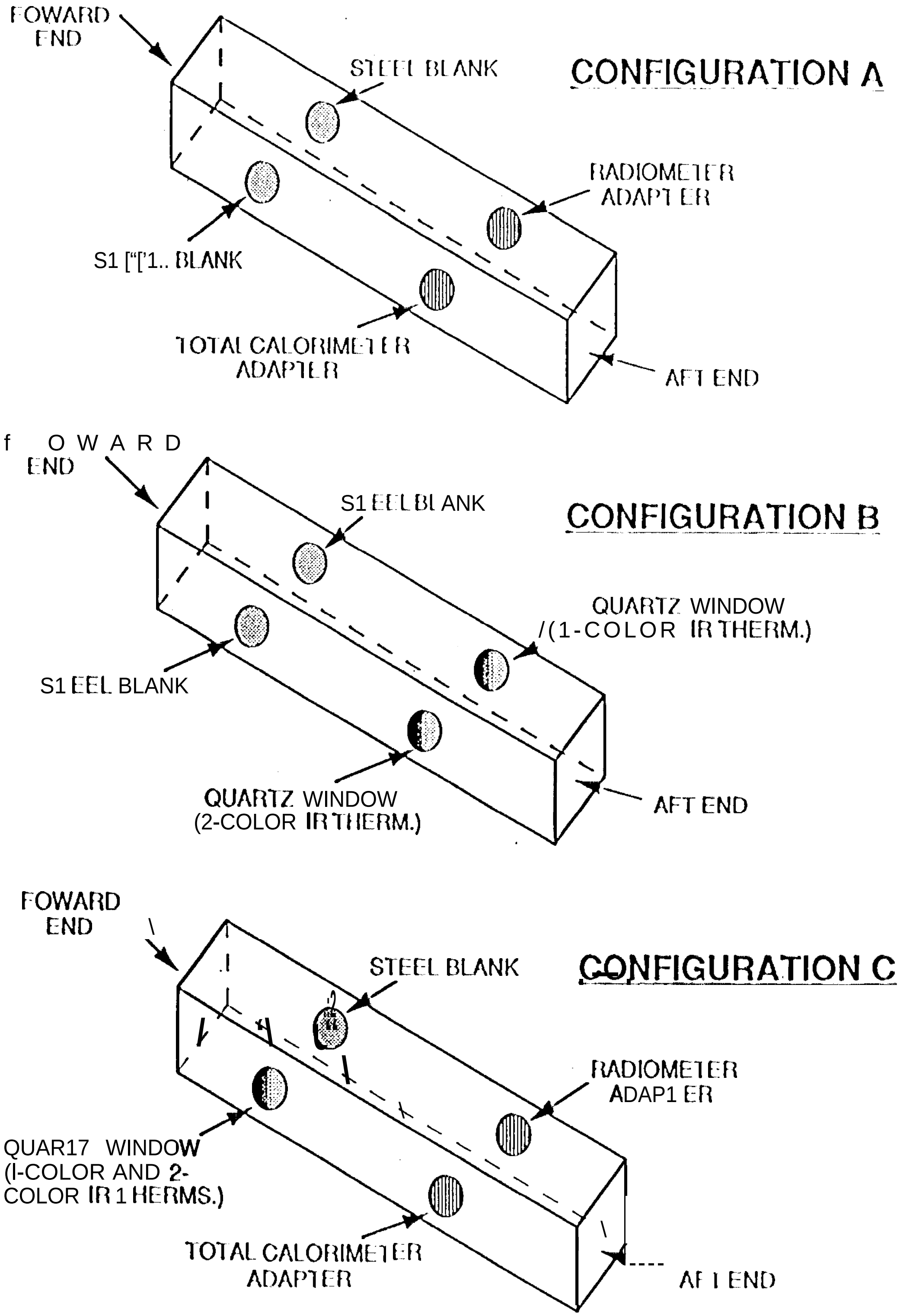

Fig. 3 Test configurations

A 1 lyCal water-cooled asymptotic calorimeter and radiometer were mounted 90° to the fuel slab surfaces. Adapters allowed them to be mounted in the aft window ports such that their sensing surfaces were flush with the walls of the combustor. Calorimeters with two different full-scale ranges were used - zero to 1 '/S 1 BTU/ft^2-s, good up to an extrapolated indicated total flux of about 350 BTU/ft^2-s (95 cal/cm^2-s), and a zero to 1000 BTU/ft^2-s (270 cal/cm^2-s) unit. Nominal response times are 50 ms and 180 ms for the calorimeter and radiometer, respectively.

Test Results

Fuel Regression Rates

Additional fuel regression rate data were obtained in association with the measurements of temperatures and heat fluxes. The time-averaged rates were determined by both before anti after measurement and weighing of the fuel slabs. Results are shown in Figures 4 and 5, together with analytical mode] calculated results published previously.[7]

The model is based on the classical dependence of regression x-ate rate on convective heat transfer in the turbulent boundary layer, and is in reasonably good agreement with the measured results. The data, the weight results in particular, show a somewhat higher dependence on G than predicted by the model and also the reduced dependence on G at the upper test values reported previously.[8] No clear effect of pressure is indicated over the pressure range tested.

Temperature Measurements

An example of the temperature measurements is displayed in Figure 6. The two IR thermometers initially read the null values shown, 600°F (588°K) and ? 100°F (1420°K) for the fuel surface and the gas temperature, respectively. The initial temperature rise is due to the methane/oxygen ignition system. At 0.5 sec. methane flow is terminated, the oxygen flow rate is raised to its operational level, and the gas temperature and fuel sur-face rise to their equilibrium values. More will be said about the gas temperatures later, in discussing heat fluxes and C* efficiency.

The fuel surface temperature data and regression rate data were used to construct an Arrhenius plot, shown in Figure 7, together with a correlation of literature pyrolysis data for an 11'1'1'11 polymer.[9,10] Data taken at the design conditions are shown as circular points and, in addition, a ballistic analysis was applied to the period of igniter opt] ation to deduce the lower regression rates existing at that time (the squares). It is believed that a majority of the data lie somewhat below the line because of the differences in the amount of carbon opacifier contained in the HTPB fuels used in the earlier and present studies, 3% and O.? 5°/0, respectively.

The pyrolysis kinetics is an element of the analytical model. These data were used to adjust the kinetics constants in the model to represent the observed higher surface temperature for a given rate, as compared to the. classical pyrolysis data

Fig. 4 Fuel mean regression rate vs oxidizer head-end mass flux, measurement results

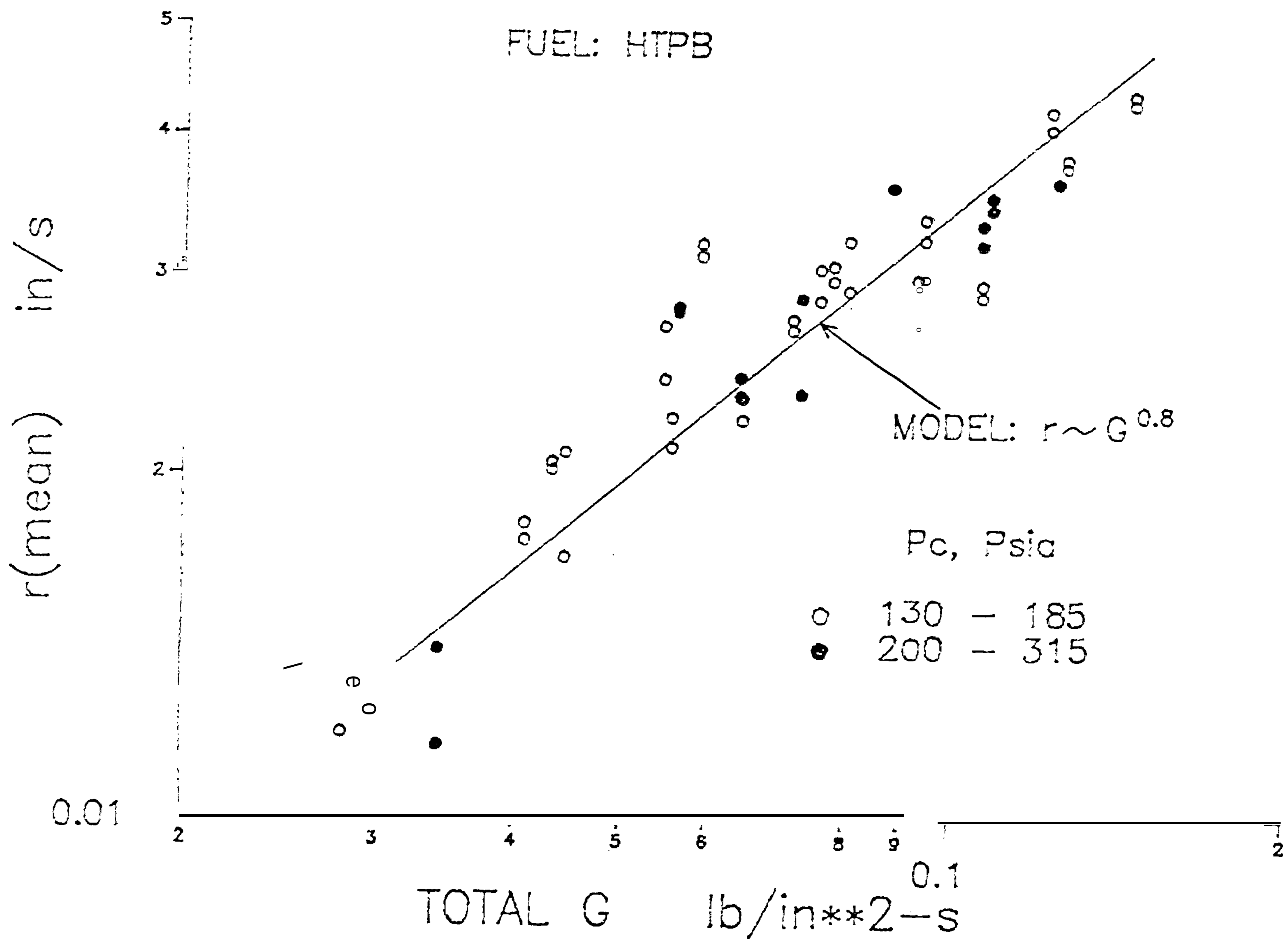

Fig. 5 Fuel mean regression rate vs. oxidizer head-end mass flux, weights results

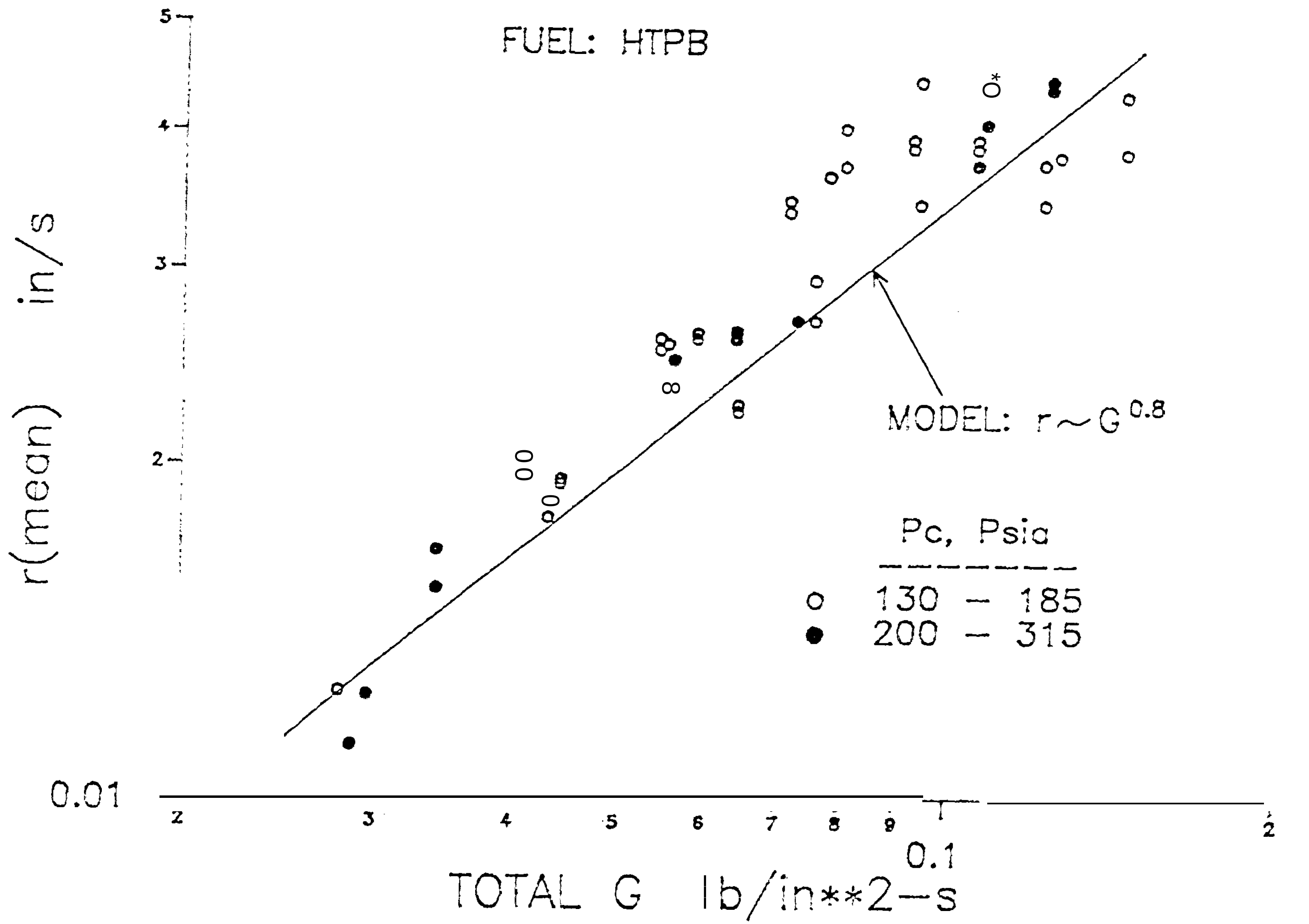

Fig. 6 Temperature vs. time

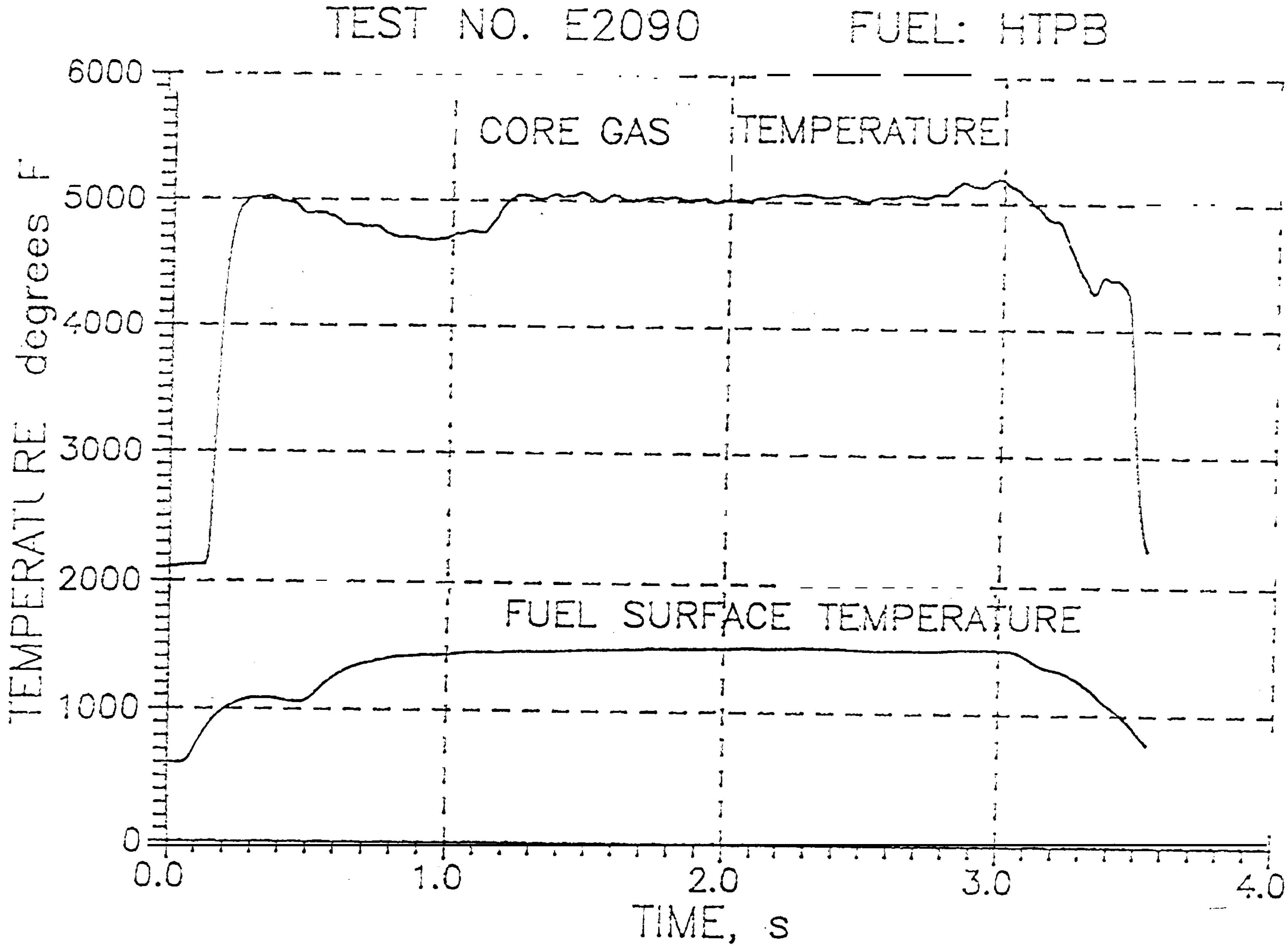

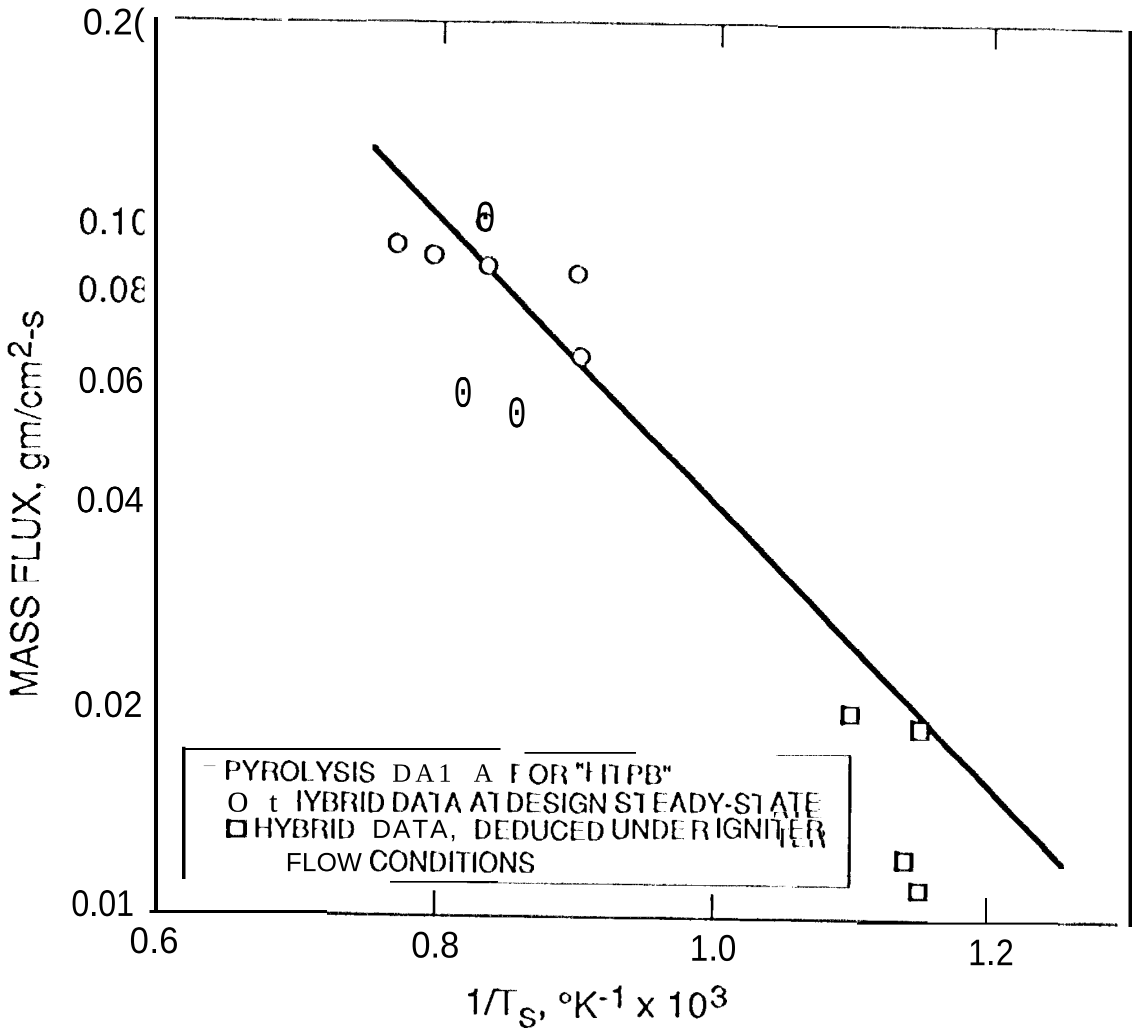

Fig. 7 Comparison of JPL HTPB hybrid fuel regression rate kinetics with literature pyrolysis data for HTPB

Heat Flux Measurements

Figure 8 shows an example of the tracking of the total heat flux and pressure data, and Figure 9 compares the total and radiation heat fluxes for the same test. Note, from Figure 8, that there is a reasonably finite time of steady-state igniter operation to enable use to be made of that data as discussed for the temperature measurements. Upon increasing the oxygen flow rate, following termination of the igniter, there are immediate responses in both total heat flux and pressure, whereas the radiation component of the heating takes a longer time to build up. The initial spike in the convection flux did not occur on every test, i.e., it appears to be a random phenomenon. Note the rise in total and radiation heat flux, chamber pressure, and core gas temperature immediately prior to termination of the test There was no corresponding increase in oxygen injection flow rate to account for it. A possible explanation will be discussed later in the section on irregular combustion. The observed fluctuations in total (convective component) heat flux are typical for these tests and will also be discussed later.

Significance of the Heat Flux Results

Radiation Component

Figure 10 displays the radiation heat flux data together with results of sets of calculations from the analytical model. Data and calculations under the igniter flow rate conditions are included, appearing at the very low pressures.

Radiation from the gas is given by:

$$\Phi_{R,g} = \sigma T_g^4 (1 - e^{-a_g P L}) \qquad (1)$$

The exponential constant, a_g, in the expression for gas emissivity is described by an empirical expression obtained from radiation measurements of the combustion products of a high-energy nonaluminized solid propellant[11]

$$a_g = 9.33 \times 10^{-4} - 6.19 \times 10^{-6} P + 1.79 \times 10^{-8} P^2$$

Calculations are shown for both theoretical and measured gas temperatures, using the radiation path length (L) as seen by the radiometer. It is observed that the model significantly underestimates the radiation heat flux based on the measured gas temperatures. Using the higher theoretical gas temperatures, the model still underestimates the radiation at the lower pressures, but overestimates the radiation at the higher pressures. These results are significant to the mechanistic analysis because they indicate that the heat transfer driving the combustion is not being properly represented in the model.

The magnitude and trend of the data suggest that there is a radiation contribution from a particle cloud, which has been previously neglected in models of nonaluminized fuels.[3,4] Videos of the tests showed extremely bright whitenesses emanating from the combustor window and exhaust plume. Post-test examinations of the burner revealed deposits of an extremely fine powdery soot. A sample of this soot was studied under a scanning electron microscope, and was found to consist of carbon particles < 0.1 μm in size. Such particles would be highly effective blackbody emitters.

Fig. 8 Total heat flux and pressure vs. time

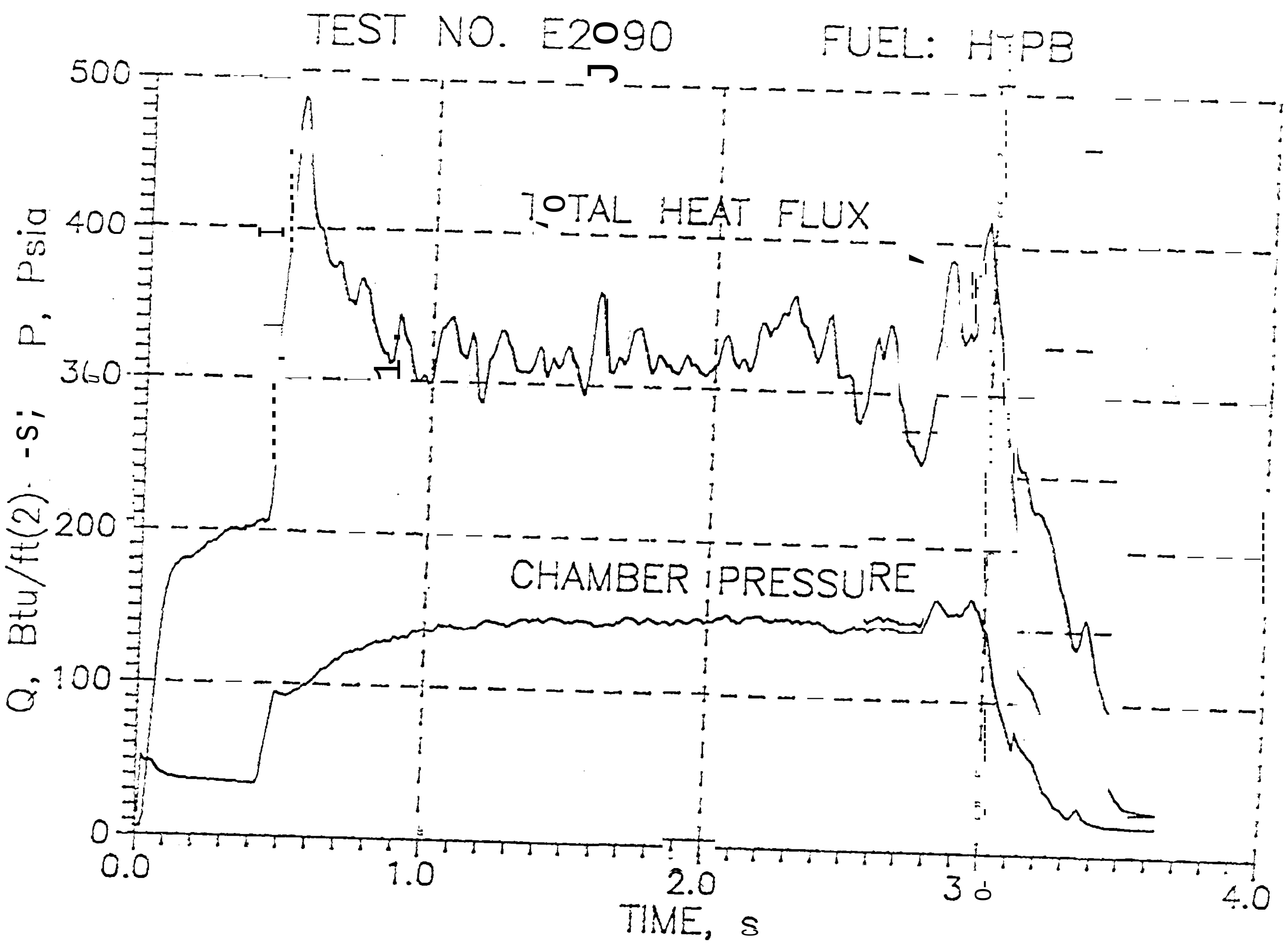

Fig. 9 Heat flux vs. time

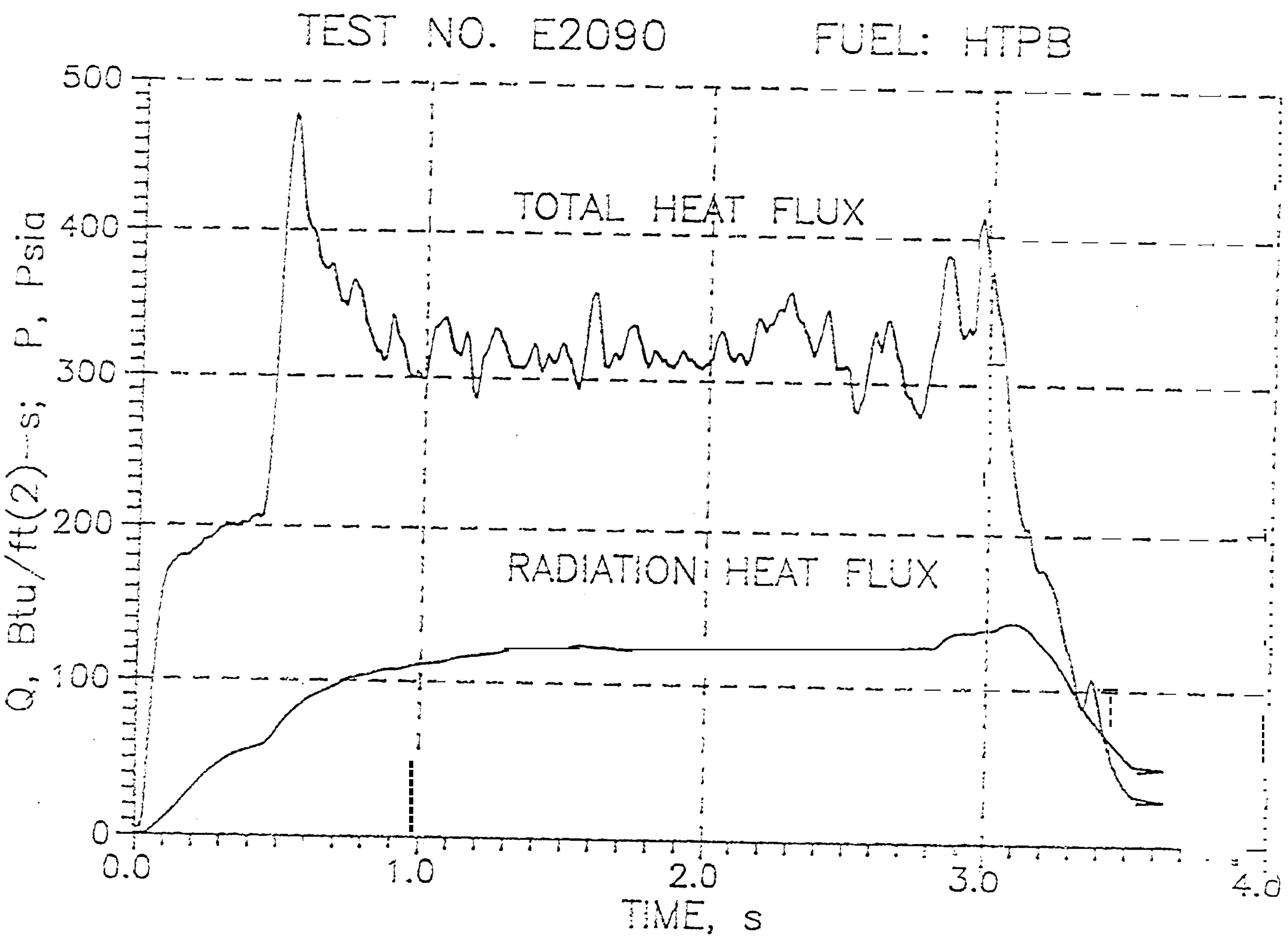

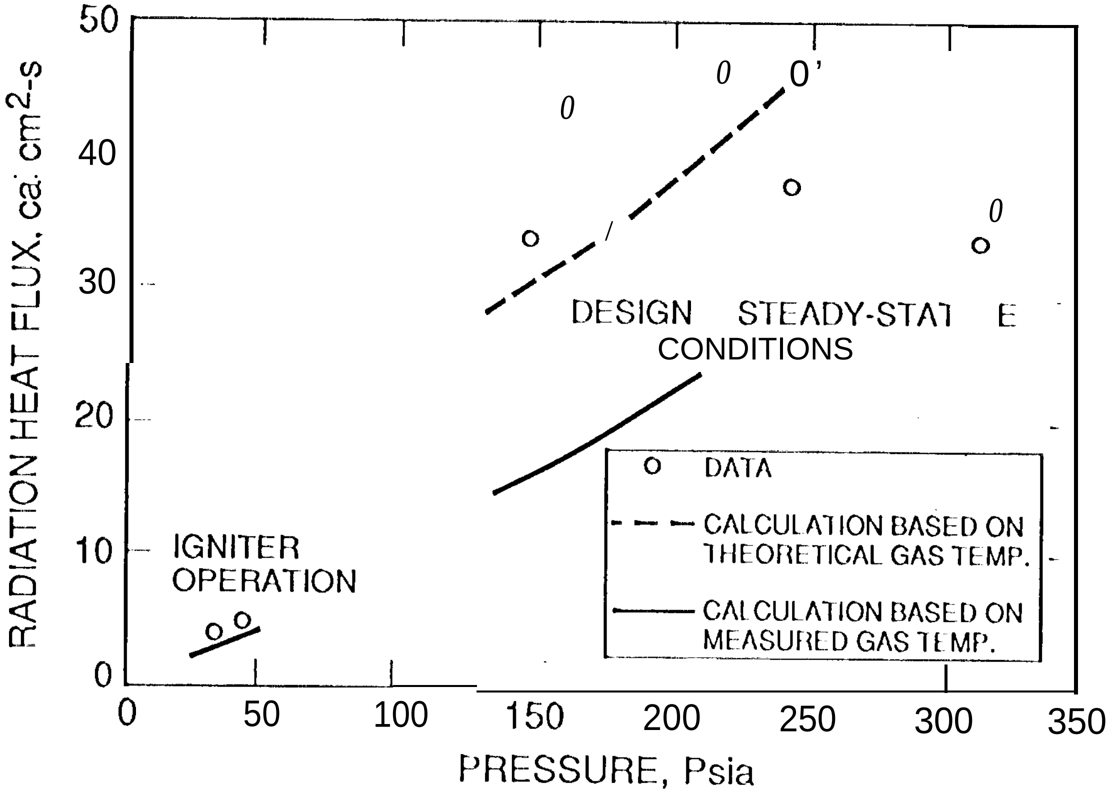

Fig 10 Radiation heat flux vs. pressure

Radiation from a particle cloud is given by:

$$\phi_{R,p} = \sigma T_p^4 \left(1 - e^{-a_p N_p}\right) \tag{2}$$

The datum point at 158 psi (1.1 MPa) was combined with an expression for particle number density to yield the following expression for the exponential constant in this expression:

$$a_p N_p = 0.134 \frac{\alpha_p P}{1 + O/F - \alpha_p} \tag{3}$$

An assumption had to be made shout the particle concentration in the gas. Reference was made to an analysis of HTPB decomposition that was performed for solid rocket exhaust plume studies using low smoke propellants.[12] On this basis, it was estimated that the baseline particle weight fraction, α_p, could be 0.045 at this reference point.

From the foregoing expressions for emissivities, it would be expected that the radiation would increase with pressure (because of increasing molecular and particle number densities). But the data at the design conditions of the tests show a decrease or peak in radiation with increasing pressure. Some other factor has come into play, which turns out to have important implications for regression rate analysis and scaling.

The tests as a group covered a broad range of O/F ratios in order to achieve the desired specific flow rates and pressures. Tests at the higher pressures tended to operate at higher O/F ratios, While the four tests below 250 psi (1.75 MPa) on Figure 10 operated at O/F ratios of about 2, the two highest pressure tests operated at O/F ratios in excess of 3. An O/F ratio of 2 is close to stoichiometry, a value of 3 is well on the oxidizer-rich side. Thus it can be expected that gas temperatures decreased somewhat at the highest pressures (measured gas temperatures were limited to the pressure range shown by the solid curve, so values at higher pressures are uncertain). Radiation is sensitive to temperature. Moreover, it can be expected that the mix of combustion products changed under the more oxidizer-rich conditions, so that emissivities were affected also.

It is plausible that less soot would be produced at higher values of O/F ratio and pressure. Starting with the baseline 158 psi condition, an estimate was made of the decrease in particle concentration needed to account for the decreased radiation at higher pressures. It was assumed that the gas temperatures at the higher O/F ratios decreased in proportion to the theoretical decrease. The result was a particle weight fraction of about 0.01. Since the particles are submicron, it is enough to provide a significant, though decreased, amount of radiation. If this effect is primarily one of O/F ratio, not pressure, the radiation would continue to be significant in large boosters designed to operate near stoichiometry.

The model calculations used in constructing Figure 4 did not account for particle radiation or changes in O/F ratio. The apparent absence of a pressure effect in the regression rate data seemed to confirm that radiation was unimportant (as calculated from the gas only, at the thinner path length seen by the fuel slabs), and temperature changes with O/F would not be enough to significantly affect the convective heating dependence upon G. Thus the model result was dominated by the classical convective heating law. It is now evident that the good agreement of the model with data (Figure 4) was a fortuity. Particle radiation can be an important factor in nonmetallized fuels, and its variation with changes in the test variables needs to be accounted for.

Convection Component

In order for the model to be closely aligned with the data (Figure 4), there must have been errors in the convective component of the heating to compensate for neglect of the particle radiation and its variations with test conditions. This was indeed the case, as shown by Figure 11, The figure displays the convective heat flux data together with calculated results for the theoretical and measured gas temperatures. The flagged data points were corrected to compensate for the fact that they were beyond the linear extrapolation range of the lower range c.ale) imeter. Data from the low flow rate igniter operation are also included.

The convective heat flux used in the model (as seen by the calorimeter gauge, in the absence of surface transpiration) is expressed by:

$$\Phi_c = \frac{0.03\ G^{0.8}}{(x/\mu_g)^{0.2}\ P_r^{2/3}}\ c_g\ (T_g - T_s)$$

Under the steady-state conditions of the tests, the calculated convective heating using the theoretical gas temperature is too high at the lower values of G. Using the measured gas temperatures, the calculated convective heating is too low at the higher values of G. Conditions where the model overestimated the convection correspond to those where it underestimated the radiation. The igniter data line up with the test data that fall along the lines of the theory using the measured gas temperatures.

Correlation of Total Heat Flux with Regression Rate

Since regression rate is a product of the response of the fuel to the sum total of the heating imposed, and there appeared to be compensating discrepancies between the model and data regarding the components of the heating, it was deemed useful to compare plots of regression rate and total heat flux. This comparison is shown in Figure 12. It is observed that there is good correlation in the G-dependence for the total heat flux and regression rate.

The scatter in the data shown in Figure 12, taken together with differences between the model and data regarding regression rates and components of heat flux, raise an important point. Part of what seems to be data scatter and discrepancy from theory may actually be variations in properties from test to test that have not been accounted for in using the theory. These include variations in radiation and gas composition that change with O/F ratio and pressure. While it would be complicated to include these effects in plots of data and theory meant to show the basic G-dependence, they should be accounted for when interpreting individual tests and in making predictions or scaling, because O/F ratio and pressure do change along with changes in G in the course of development programs and tests.

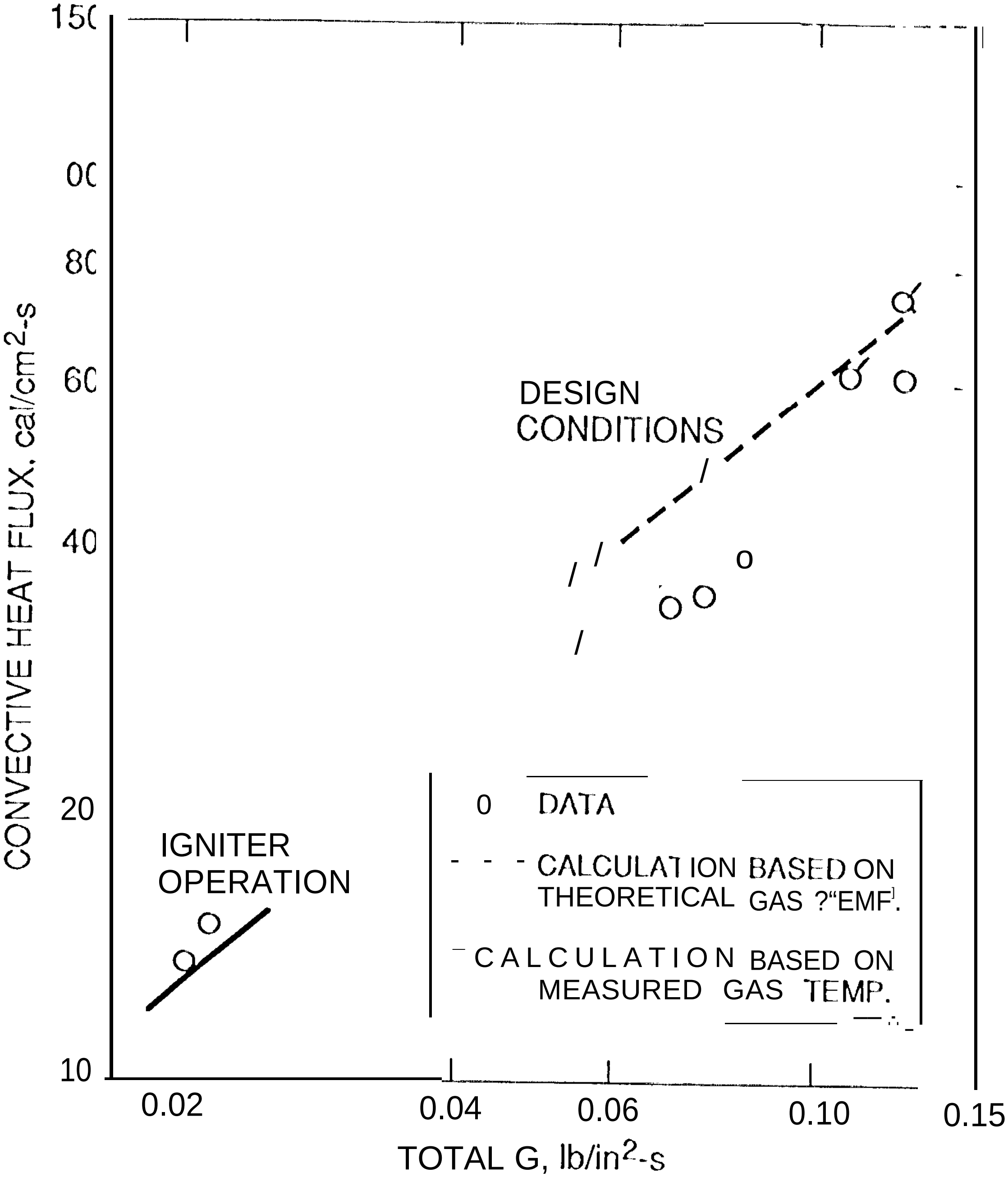

Fig. 11 Convective heat flux vs. total mass flux

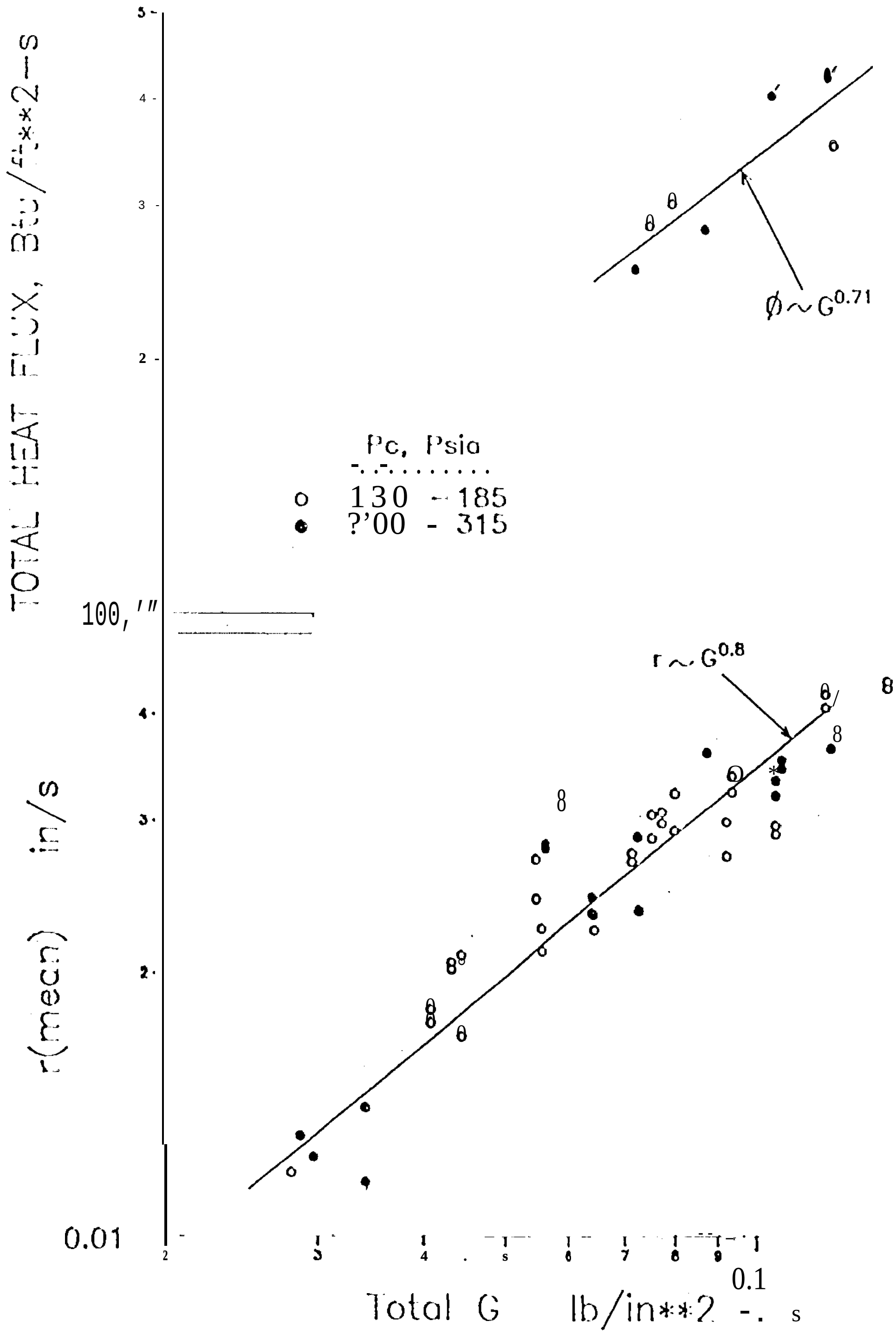

Fig. 12 Comparison of regression rate and total heat flux variations vs. total mass flux

Significantly, there has not been a single regression late expression that explicitly includes O/F ratio (whether analytical or empirical), and only a few include pressure (even for metallized fuels).[4] Thus it should not be surprising that statistical variations as high as 16% have been found when applied aposteriori to correlate existing data, and as high as 74% when applied a priori to predict or scale regression rates.[4]

A final point is that these slab combustor tests have now reached a G level that touches the low end of the range encountered on the JIRAD program[13]

Combustion Efficiency

C* efficiency was measured in the course of the series of tests. A factor enhancing the accuracy of the results is the absence of nozzle throat erosion (a significant source of C* uncertainty when present in solid rocket motor tests). It was found that C* efficiency was low at low pressures (below about 200 psi (1.4 MPa)) or at low O/F ratios (below about 1.7, on the fuel-rich side of the stoichiometric value of 2..0).

Plots of C* efficiency versus pressure and O/F ratio are shown in Figures 13 and 14, respectively. For the sake of clarity, the low efficiencies at low O/F ratio are excluded from Figure 13 and the low values at low pressure are excluded from Figure 14. Thus Figure 13 shows the effect of pressure at favorable O/F, and Figure 14 shows the effect of O/F at favorable pressures.

The efficiency increases with pressure, as would be expected, but is at higher levels than might be expected considering that there are no special mixing aids and a lalmato~-y-scale test device is used. It is possible that the concern about combustion efficiency with hybrids has actually been a question of efficient liquid atomization and not one of fuel-oxidizer mixing. Significantly, these tests employed gaseous oxygen as the injectant. If this assertion is true, then future motor developments should concentrate on the injectant system for the liquid oxygen more so than on aft end motor arrangements for mixing. Prior needs for such mixing arrangements may have been a consequence of the liquid atomization rather than the boundary layer process per se. The costs of more sophistication in the liquid injection may be worth the potential weight and space savings in the motor, and may also be helpful to stability of operation.

Figure 14 is interesting because it shows that efficiency remains high on the oxidizer-rich side of stoichiometry, but falls off rapidly on the fuel-rich side. A plot of the theoretical thermochemical temperature is included to explain this result. Note that the temperature is at a peak near stoichiometry, remains high on the oxidizer-rich side and falls off on the fuel-rich side. This suggests a kinetics rather than mixing limitation on the combustion of the gases in the burner cavity, which supports the above assertion that mixing per se may not have been the problem with efficiencies in hybrids, but rather more attention should be given to liquid atomization. Figure 14 data also suggest that O/F excursions in a motor design should center on oxidizer-richness in order to avoid fuel-rich regions. This information could be worth considerable delivered performance points.

For completeness, the measured core gas temperatures are also shown on Figure 14.

Figure 15 presents a correlation of measured C* efficiency with measured gas temperature efficiency. Since the square root of temperature appears in the definition of C*, the temperature efficiency is expressed in terms

Fig 13 C* efficiency vs. pressure for O/F ratio ≥ stoichiometry

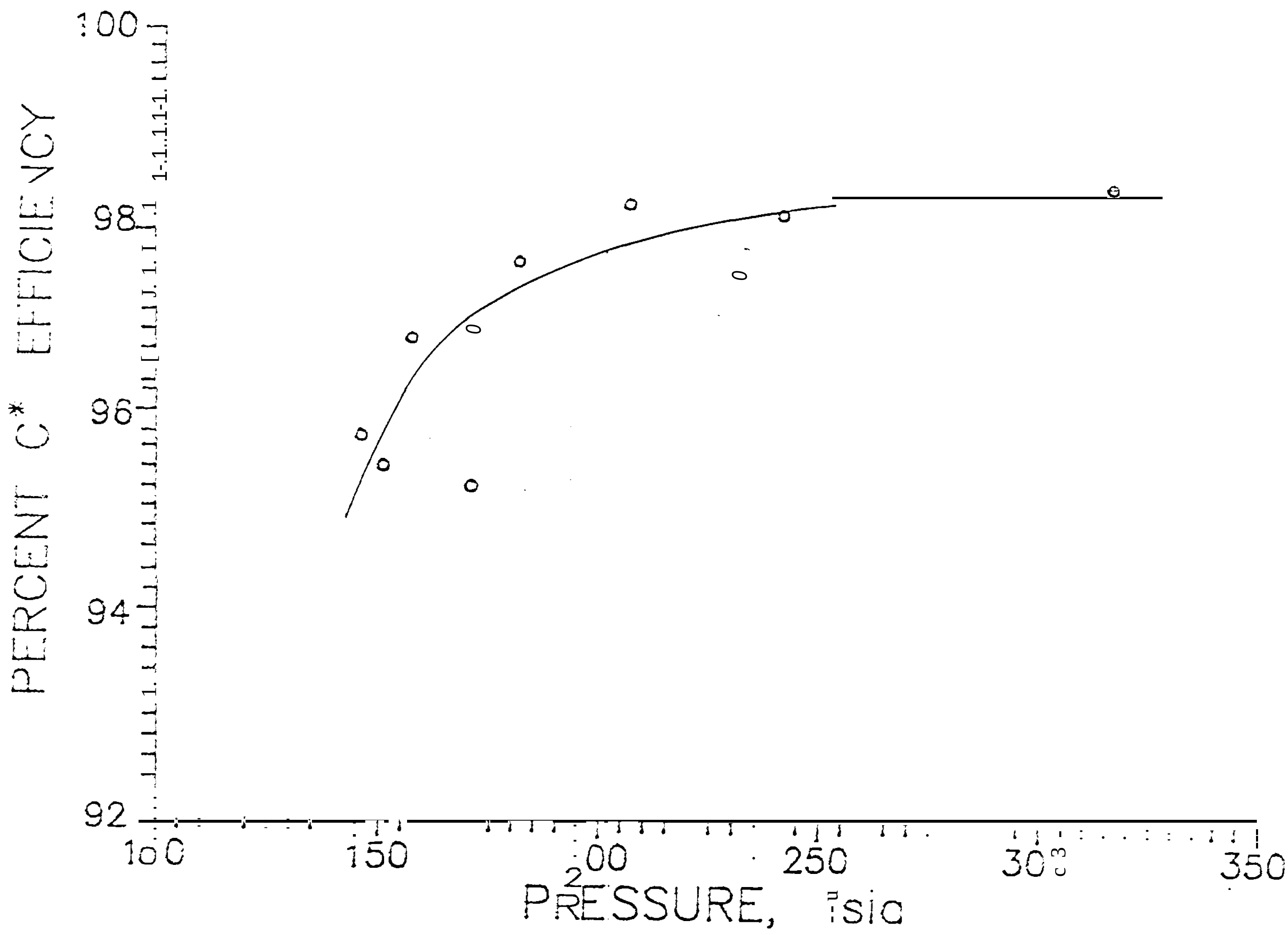

Fig 14 C* efficiency and gas temperature vs. O/F ratio

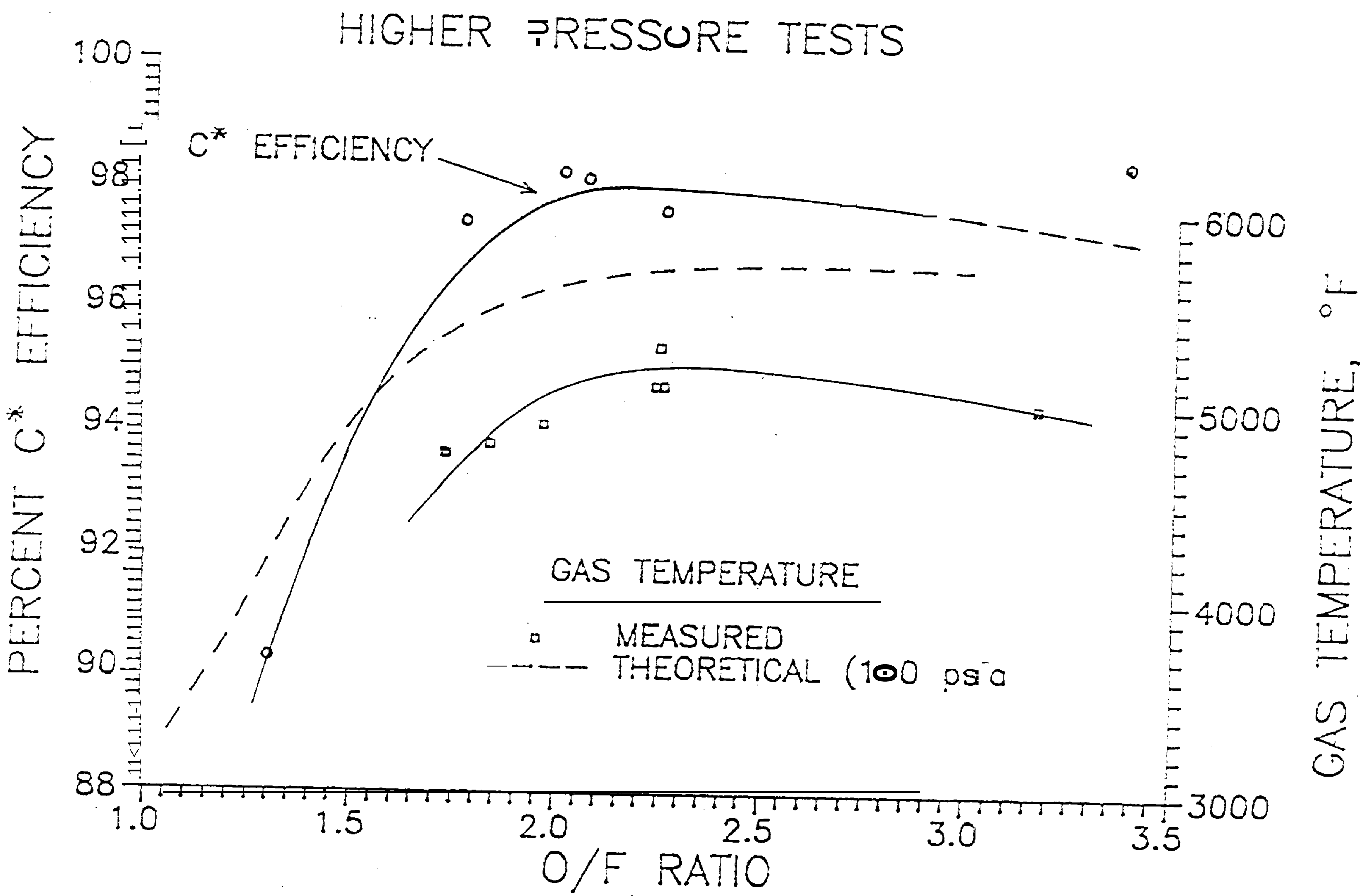

Fig 15 Measured C* efficiency vs. measured gas temperature efficiency

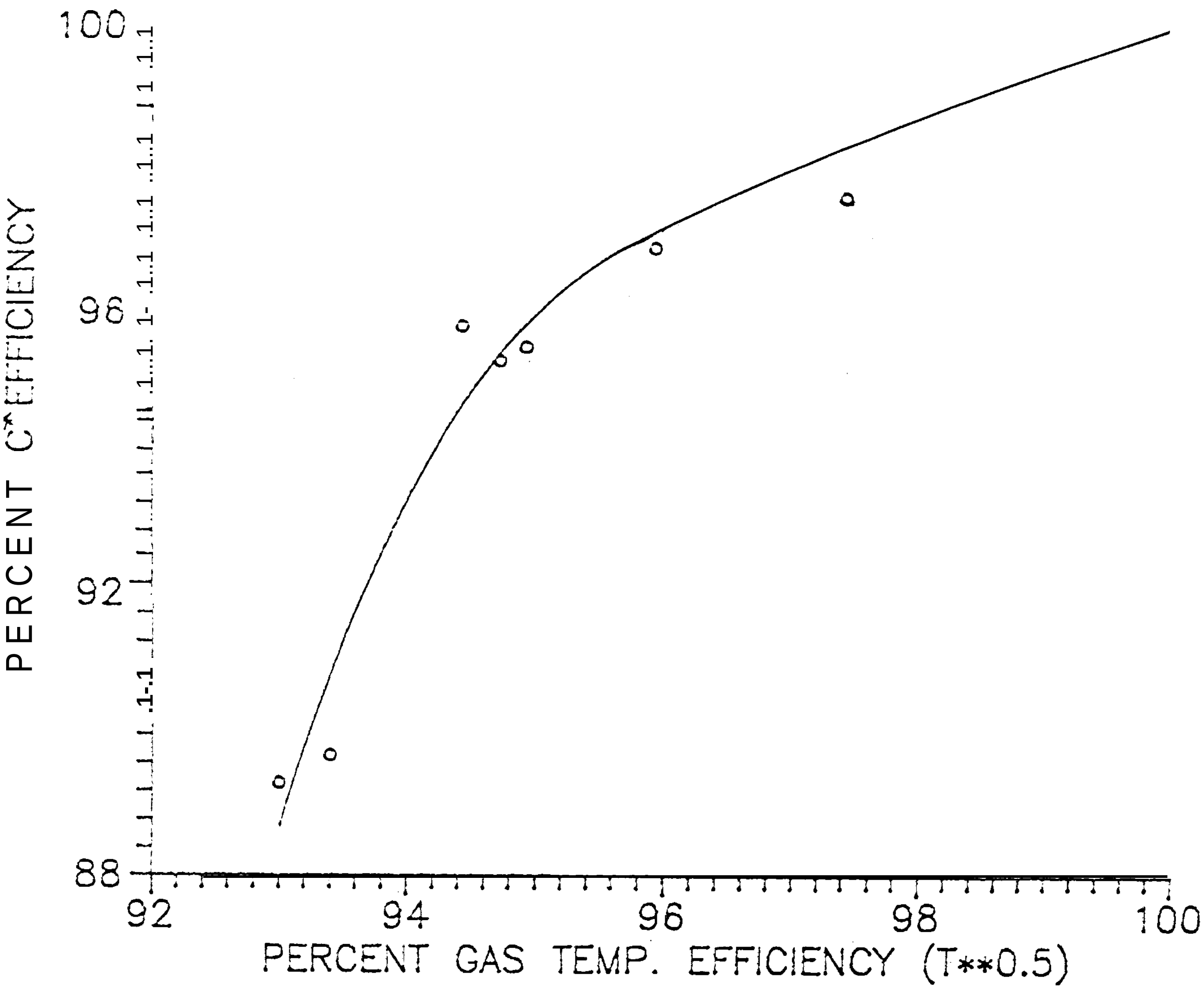

of the square root of temperature ratio. The curve fit to the data assumes 1000/0 C* efficiency at 100'% gas temperature efficiency, by definition. The correlation was made as a check on the credibility of the temperature data, which appears validated, and also to show the sensitivity of C* efficiency to temperature regarding the importance of kinetics. The high initial slope of the correlation indeed shows that C* efficiency is sensitive to the temperature developed by the combustion Since this is a vicious circle type of process, the more favorable the O/F ratio for higher temperature capability, the better the delivered performance.

Irregular Combustion

The total heat flux exhibited a modulation in amplitude that bore, in many cases, a rough correlation with the 3 to 4 Hz oscillations in pressure often observed in these tests,[7] with the more rapid time-response pressure signal oscillations leading in phase. Figure 16 shows a case where, at a burn time of 2.1 sec., there was a distinct rise in the mean pressure level, with superimposed higher frequency oscillations (-30 Hz, still well below the acoustic range). A comparable step increase in mean total heat flux (-40%) and approximately 20001: (365 "K) increase in gas temperature occurred. The rate of oxygen injection remained constant. The phenomenon (d.c. shift in mean pressure with onset of instability) has the appearance of the rectification that occurs in acoustic velocity-coupled instability in solid propellant rockets.[14]

These observations support the earlier postulation[8] that the driving mechanism for the exhibited sub-acoustic pressure irregularities is some type of flow-combustion turbulence interaction along the surface of the fuel/propellant slab.

Conclusions

1. Any model of the hybrid motor ignition process will have to be able to describe the progression of the fuel surface temperature-time profile, as observed in these experiments.

2. The measured fuel surface temperature data were in fair agreement with literature pyrolysis data for 11'1'1'11. A probable explanation for the difference is the higher concentration of carbon opacifier contained in the HTPB for the latter.

3. Particle radiation from fine powdery soot is a significant contributor to the heat flux driving the regression rate of a pulc11'1'1)11 fuel, and should be accounted for in future applications of the analytical model to predict regression rates and scaling.

4. For the most part, measured convective heat flux is consistent with the turbulent boundary layer law that is the primary mechanism for driving regression rate. To the extent that there is a discrepancy, an adjustment could be made to the value of the convection coefficient in the model. More data is needed at higher values of flow rate (G) and pressure.

5. The G-dependence of regression rate is consistent with that of the total heat flux imparted by the combustion products and flow environment

6. While data scatter in plots of regression rate vs. G may be due in part to vagaries in hybrid fuel combustion, it is believed that it is also due to

Fig. 16 Chamber pressure vs. time

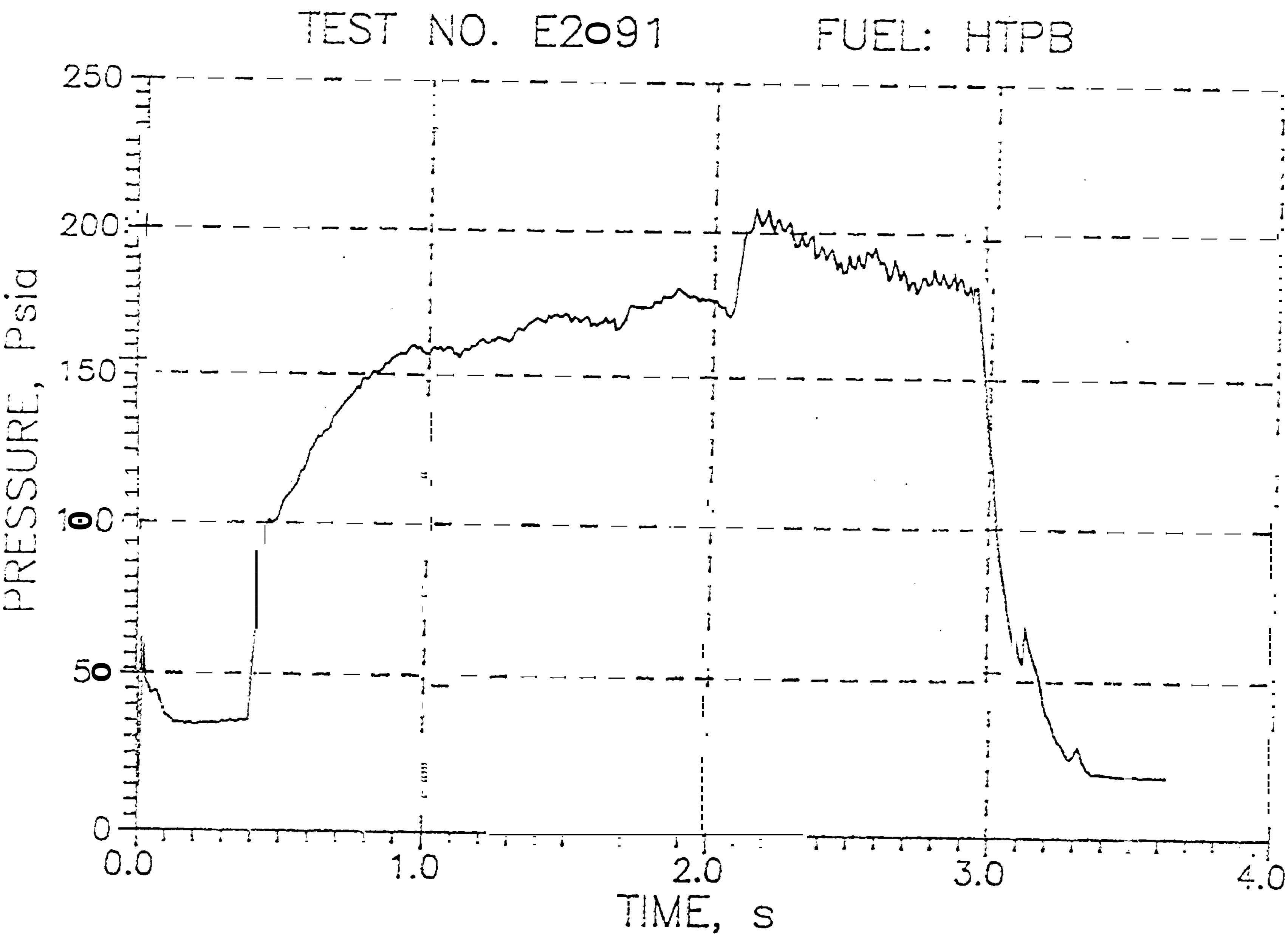

variations in gas properties and radiation as affected by variations in O/F ratio and pressure. Further, it is believed that failure to account for these changes in models and empirical correlations is a reason for statistical variations in the data and errors in predictions and scaling. Future analytical efforts should try to account for these variations and possibly exploit them to improve regression rate properties.

7. Combustion efficiency of11'1'1'11 with gaseous oxygen in a laboratory-scale combustor is surprisingly good at pressures above 200 psi (1.4 Mpa) and at O/F ratios that are not too fuel-rich. The maintenance of high efficiency under oxidizer-rich conditions and the sharp drop-off with fuel-richness suggests the manner to handle O/F excursions in a design to improve performance. Correlation of efficiency with the temperature of the environment, and the achievement of good efficiency with gaseous oxygen, suggest that fuel/oxidizer mixing has not been the limiting problem in hybrid efficiencies. Rather, more attention should be given to liquid atomization, and adequate temperatures to enhance kinetics.

Acknowledgments

The assistance of the Technical Operations personnel at the J}'] , Edwards Facility in performing the slab combustor experiments is gratefully acknowledged

The research described in this paper was carried out at the Jet Propulsion Laboratory, California Institute of Technology, under contract with the National Aeronautics and Space Administration

References

1. Kuentzmann, 1'. and Sternfeld, 11. J., "What Future for Hybrid Rocket Propulsion?", European Space Agency, Bordeaux, France, June 1991.

2. "What is the Future of Hybrid Rocket Propulsion for 11, S. Space Launch Systems?", Position Paper by the National Space Propulsion Synergy Group, 199'2 draft

3. Netzer, 1). W., "Hybrid Rocket Internal Ballistics," CPIA Publication No. 222, Naval Postgraduate School, Monterey, CA, Jan. 1972.

4. Estey, 1'., Altman, D., and McFarlene, J., "An Evaluation of Scaling Effects for Hybrid Rocket Motors", Paper No. AIAA 91-2517, AIAA/SAE/ASME 27th Joint Propulsion Conference, Sacramento, CA, June 1991.

5. Strand, 1,., et al., "Hybrid Rocket Fuel Combustion and Regression Rate Study", Paper No. AIAA 92-3302, AIAA/SAE/ASME/ASEE 28th Joint Propulsion Conference, Nashville, TN, July 1992.

6. Strand, L. I). and Cohen, N. S., "Hybrid Rocket Fuel Combustion Study", 29th JANNAF Combustion Subcommittee Meeting, CPIA Publ. 593, Vol. 11, Oct 199?, pp. 149-1s4.

7. Strand, L. D., Ray, R L., and Cohen, N. S., "Hybrid Rocket Combustion Study", Paper No. AIAA 93-2A 12, AIAA/SAE/ASME/ASEE 29th Joint Propulsion Conference, Monterey, CA, June 1993.

8. Cohen, N. S. and Strand, L. D., "Hybrid Propulsion Based on Fluid-Controlled Solid Gas Generators", Paper No. AIAA 93-2550, AIAA/SAE/ASME/ASEE 29th Joint Propulsion Conference, Monterey, CA, June 1993,

9. Cohen, N. S., Fleming, R W., and Derr, R L., "Role of Binders in Solid Propellant Combustion", AIAA J., Vol. 12, Feb. 1974, pp. 212-218.

10. Lengelle, G., et al., "Condensed Phase Behavior and Ablation Rates of fuels for Hybrid Propulsion", Paper No. AIAA 93-24 13, AIAA/SAE/ASME/ASEE 29th Joint Propulsion Conference, Monterey, CA, June 1993.

11. Cohen, N. S., "Ballistic Predictions for Mass-Augmented Solid Rocket Motors", Report AFRPL-TR-71 -133, Lockheed Propulsion Co., Redlands, CA, Dec. 1971.

12. Cohen, N. S. and McGrath, D. K., "Nonequilibrium Thermochemistry Studies", 23rd JANNAF Combustion Meeting, CPIA Publ. 457, Vol. 2, Oct. 1986, pp. 63-71.

13. Boardman, T. A., et al., "Development and Testing of 11- and 24-Inch Hybrid Motors Under the Joint IR&D Program", Paper No. AIAA 93-2552, AIAA/SAE/ASME/ASEE 29th Joint Propulsion Conference, Monterey, CA, June. 1993.

14. Culick, F. E. C., "An Introduction to Velocity Coupling in Solid Propellant Rockets", NWC TP 6363, Naval Weapons Center, China Lake, CA, Feb. 1983.